JOURNAL OF Materials CHEMISTRY

Microporous layered tin sulfide, SnS-1: molecular sieve or intercalant?

Carol L. Bowes,[a] Srebri Petrov,[a] Greg Vovk,[a] David Young,[a] Geoffrey A. Ozin*[a] and Robert L. Bedard[b]

[a]*Materials Chemistry Research Group, Lash Miller Chemical Laboratories, University of Toronto, 80 St. George St., Toronto, Canada, M5S 3H6*

[b]*UOP Research and Development, 50 East Algonquin Road, Des Plaines, IL, 60017-5017, USA*

The results of a detailed study of the structure, thermal/pressure stability, ion-exchange, amine intercalation and adsorption property relations, of microporous layered tin(IV) sulfides $A_2Sn_3S_7$, denoted SnS-1, where A = tetramethylammonium (TMA), quinuclidinium (QUIN), or *tert*-butylammonium (TBA), are reported and comparisons are made to zeolites and layered metal sulfides. The thermal stability of the materials indicates potential for the removal of void filling organic template without affecting the integrity of the lattice. The sensitivity of the materials to applied pressure is found to depend on the nature of the occluded template. Aqueous ion-exchange and gas-phase exchange by amines are observed in SnS-1 templated with the tertiary ammonium cation. This allows for an intercalation-like process similar to the layered chalcogenides. Adsorption isotherms for SnS-1 show it to exclude gaseous species of kinetic diameter >3.4 Å, thus acting as a molecular sieve like zeolites and showing potential for catalysis, separation and chemical sensing applications.

Introduction

Since a group of hydrothermally synthesized and templated microporous germanium(IV) and tin(IV) sulfides was reported in 1989,[1] the class of microporous layered tin(IV) chalcogenides has expanded and received a great deal of attention. In particular, the topology of $A_2Sn_3X_7$ (A = cation), denoted SnX-1, where X = S, Se and R represents an organic void filler, has been characterized structurally through single crystal X-ray diffraction.[2] This phase has remarkable framework flexibility and is responsive to adsorbed guests.[3] The mode of formation and high-temperature thermochemistry of SnS-1 have been reported.[4] High resolution images of the crystal surfaces obtained through AFM microscopy have been published,[5] and the synthesis and characterization of a series of tunable composition isostructural thioselenide materials, SnSSe-1, have been studied.[2] Alternative syntheses of all-inorganic Cs-SnS-1 have been reported[6] and real time synchrotron PXRD studies of the synthesis of SnS-1 have contributed to the understanding of the mechanism of its formation.[7] Recently, adsorption and electrical conductivity data have shown the material to have potential for chemical sensing.[8a,b] As a break from the conventional use of hydrothermal synthesis conditions to microporous layered tin(IV) sulfides, a very soft room temperature methodology has been disclosed for preparing SnS-1 materials that utilizes controlled assembly of $Sn_2S_6^{4-}$ modular units.[8c] The effect of a microgravity environment on the self-assembly of SnS-1 has also been investigated.[8d]

In classifying the properties of SnS-1 it is necessary to compare it to other materials. Being a microporous layered metal chalcogenide, it might be related to layered materials like SnS_2, berndtite, whereas having a microporous structure it might more resemble a zeolitic material. Berndtite is a layered material similar in many respects to the extensively researched transition metal dichalcogenides.[9,10] The layers consist of tin(IV), occupying quasi-octahedral sites between two layers of hexagonal-close-packed sulfur(−II) atoms. These layers are then stacked orthogonal to the ***c***-axis with a spacing of 5.928 Å.[11] Differences in layer stacking sequence lead to more than 70 polytypes.[12] As the layers are held together by van der Waals forces, the solid readily expands by 100% or more[13] along ***c*** to intercalate for example, pyridine, cobaltocene, or alkali metals.[11,14] It is stable to high temperature, 800 °C in inert atmosphere, but on exposure to oxygen transforms to SnO_2, starting at 400 °C and complete by 800 °C.[15] Many of the spectroscopic studies of SnS_2 have been carried out in the extensive investigation of cobaltocene intercalation.[13,16]

Zeolites, on the other hand, are microporous aluminosilicates that are stable in air to high temperature. They are a class of molecular sieves, entirely able to adsorb and desorb other species without significant changes in their lattice parameters. These phases have pores of up to 7.4 Å.[17] They are usually stable to dehydration and/or removal of the void filler, and can undergo exchange of charge balancing cations. Zeolites are composed exclusively of tetrahedral SiO_4/AlO_4 centres, with topologies based upon four-connected three-dimensional networks. Generally, no lattice expansion comparable to layer swelling can occur and their porosity is permanent. Layered clays are also employed as molecular sieves. Typically the layers have no openings so their porosity is dependent on intercalation or pillaring.[18]

These classes of materials show the range of properties that might be expected from a microporous layered tin(IV) sulfide. In studying SnS-1 the question of where it fits in this range of behaviour is important. Does SnS-1 undergo intercalation or sieving behaviour, or both? What type of adsorption properties will it display? Will it permit removal of the organic space filler? Is it feasible to perform ion-exchange of the organic cation? In this paper a detailed characterization of SnS-1 is reported focusing attention on structure and stability, ion-exchange and adsorption behaviour, so as to address the issue of the nature of SnS-1.

Experimental

Synthesis

SnS_2 was prepared by the slow addition of an aqueous Na_2S solution to an aqueous solution of $SnCl_4 \cdot 5H_2O$. After adjusting the pH to 6.6 with NaOH, the precipitate was filtered or centrifuged, and washed with copious amounts of deionized water until no Cl^- remained in the washings. Tetramethylammonium bicarbonate, $TMAHCO_3$, was prepared by bubbling CO_2 (Matheson) through an aqueous solution of TMAOH at room temperature. Owing to an

exothermic hydroxide neutralization process the temperature of the solution rose and when it returned to room temperature the reaction was complete. Other amines, such as quinuclidine (QUIN), (Aldrich 97%), and *tert*-butylamine (TBA), (Fluka, 99.5%) were used as received. TMA-SnS-1 was synthesized from the static reaction of SnS_2 : $TMAHCO_3$: 33 H_2O at 150 °C for 7 days. QUIN-SnS-1 was prepared from SnS_2 : quinuclidine : 33 H_2O tumbling at 150 °C for 6 days. TBA-SnS-1 was prepared from SnS_2 : *tert*-butylamine : 33 H_2O at 150 °C tumbling for 7 days. Products were recovered and washed by slurrying with deionized water, centrifuging and decanting twice, or until the supernatant was clear. Samples were allowed to air dry and were stable indefinitely in air.

Characterization

Powder X-ray diffraction (PXRD) methods were used extensively to identify phases, optimize syntheses, and monitor thermally and pressure induced changes in structure and unit cell dimensions. PXRD was performed using a Siemens D-5000 diffractometer with Cu-Kα radiation ($\lambda = 1.541\,78$ Å) and a Kevex solid state detector with step sizes of typically 0.02° in 2θ and 1 s step time. Samples were prepared in flat-plate sample holders, open to the atmosphere. The Siemens D-5000 was equipped with a variable temperature stage for high temperature *in situ* studies to obtain temperature stability data and information about thermolysis products, from room temperature to 700 °C, and under various atmospheres or vacuum. FT-Raman spectroscopy (FTR) was performed at the Ontario Laser and Lightwave Research Centre on samples sealed in glass capillary tubes using a Bomems MB-157 Fourier transform spectrometer with an InGaAs near-IR detector in back-scattering mode. The Spectra Physics diode-pumped Nd : YLF laser emitted at 1064 nm with a 350 kHz repetition rate. Notch filters covering ranges 150–3750 and 40–150 cm^{-1} were used to block Rayleigh scattering. Mass spectrometry (MS) was performed on a VG 70-250S instrument, operating at an ionizing energy of 70 eV for electron impact (EI) spectra (VG Analytical, Wythenshawe, UK). The source temperature was 250 °C with a pressure in the housing of 2×10^{-6} mbar. The samples, typically 0.1 mg, were placed in a glass capillary into the Macor tip of a direct solids probe and pumped to 10^{-2} mbar before exposure to the mass spectrometer source. The temperature of the probe was ramped at 0.5 °C s^{-1}, typically from 50 to 350 °C or higher. Mass spectra were collected in a period of 1 s and repeated every 3 s. This technique was used both for studying thermolysis and for detecting the outcome of amine exchange experiments.[19] Thermogravimetry (TG) was undertaken using a Perkin-Elmer TGA7 instrument, with the sample held under flowing nitrogen with heating rates of 3–10 °C min^{-1} between 40 and 750 °C. Sample masses were typically 20 mg. In some cases, mass spectrometry was performed on the outgas of the sample to identify volatile species coming off at various temperatures. Adsorption measurements were performed using a glass vacuum McBain balance system. Samples of known mass, typically *ca.* 200 mg, were contained in a miniature quartz basket suspended from a quartz spring with 0.1 mm mg^{-1} sensitivity. Samples were dehydrated at room temperature or 120 °C for several hours at pressures below 1×10^{-5} Torr. Pressures were measured with two MKS Baratron pressure transducers with ranges covering 0–100 and 0–1000 Torr. A Schaevitz linear displacement transducer measured sample displacement (gas uptake by the sample) as gas pressure was slowly increased by flowing gas into the system though a piezoelectric valve. For argon and nitrogen measurements, a constant, small flow rate (0.2 cm^3 min^{-1}) was administered into the system, and pressure uptake data were continuously collected on the assumption that because the flow rate is so slow, the sample will always be in equilibrium with the adsorbate gas. For water and CO_2, the gas was added incrementally and manually. When equilibrium (< 1 mTorr min^{-1} change) was achieved, a point on the isotherm was recorded. The sample temperature was controlled by a refrigerant bath of liquid nitrogen for N_2 as the adsorbate or dry ice–acetone for CO_2 as the adsorbate.

Results and Discussion

The PXRD patterns of three chosen materials, tetramethylammonium-SnS-1 (TMA-SnS-1), *tert*-butylammonium-SnS-1 (TBA-SnS-1), and quinuclidinium-SnS-1 (QUIN-SnS-1), are listed in Table 1. All three may be crystallised in the orthorhombic space group $P2_12_12_1$. Raman spectroscopy has been shown to be useful in fingerprinting materials with the SnS-1 structure.[20] The diagnostic region is shown in Fig. 1, and demonstrates that SnS-1 materials can be synthesized using diverse void fillers. The three main bands observed between 250 and 400 cm^{-1}, represent the expected three Raman active local vibrational modes of the trigonal bypyramidal SnS_5 primary building block of the microporous layered SnS-1 structure.[20]

Structural characteristics of SnS-1 type materials

The microporous layered tin(IV) sulfides, SnS-1, are considered to be composed of three main structural units that control their physical and chemical properties.

(i) $(Sn_3S_7)^{2-}$ anionic microporous layers, based upon interconnected broken-cube clusters.

(ii) A^+ organic template cations, filling the voids within and between the layers, balancing the charge of the framework and supporting the whole structure. Being weakly bonded to the framework, the template has some degree of mobility, causing partial disorder in the structure. A^+ can be different and in this study only TMA, TBA and QUIN are considered. The shape and size of A^+, Table 2, is found to control the spacing between the layers as well as the thermal stability, adsorption and sieving characteristics of these materials.

(iii) Water molecules, which do not seem to be confined to certain sites in the structures. There is no evidence for a fixed number of water molecules in a particular structure. They should not be considered as a part of the structure, but as a third variable component which can influence the degree of crystallinity, thermal stability and physical rather than framework structural properties of the materials.

The following discussion on the structural relations and individual features of these materials is based on the single crystal structure determination of $TMA_2Sn_3Se_7$. It has an orthorhombic lattice ($P2_12_12_1$, $Z = 8$) with $(Sn_3Se_7)^{2-}$ layers coinciding with (020) planes.[2] There is a close structural relation between TMA-SnSe-1 and differently templated sulfides. The TMA, TBA and QUIN compounds are found to be isostructural with TMA-SnSe-1 based upon the following experimental data:

(i) $TMA_2Sn_3Se_xS_{7-x}$ materials with different Se : S ratios exhibit a linear shift of the unit cell parameters following Vegard's Law, typical for continuous isomorphic substitution.[2]

(ii) The lack of large enough single crystals in the TMA, TBA and QUIN materials has so far prevented single crystal X-ray structure determination. High resolution powder X-ray data and Rietveld refinements of these materials confirm that they are of the SnS-1 structure type. The full details of this study will be reported in a forthcoming paper.[21]

(iii) A detailed analysis and comparison of the powder data for the TMA, TBA and QUIN materials has been performed. A list of the first (mainly unique) reflections of these materials along with their calculated unit cell parameters are shown in Table 1. The reflections are given with their *d*-spacings, normalized intensities and Miller indices. All three sets of $A_2Sn_3S_7$ X-ray powder data were successfully assigned in the same

Table 1 Comparative PXRD data for different $A_2Sn_3S_7$ materials

TMA-SnSe-1			TMA-SnS-1			QUI-SnS-1			TBU-SnS-1		
$a=13.7874(40)$ Å $b=16.7477(50)$ Å $c=23.9275(78)$ Å $V=5525(2)$ Å^3			$a=13.1284(18)$ Å $b=16.7796(20)$ Å $c=22.9086(31)$ Å $V=5046(1)$ Å^3			$a=13.1019(08)$ Å $b=17.6833(13)$ Å $c=23.2022(14)$ Å $V=5421.2(4)$ Å^3			$a=13.0266(08)$ Å $b=17.5866(12)$ Å $c=23.0393(14)$ Å $V=5278.2(4)$ Å^3		
$\lvert\Delta 2\theta\rvert=0.0163$			$\lvert\Delta 2\theta\rvert=0.0053$			$\lvert\Delta 2\theta\rvert=0.0055$			$\lvert\Delta 2\theta\rvert=0.0049$		
d_{hkl}/Å	I/I_0	hkl	d_{hkl}/Å	I/I_0	hkl	d_{hkl}/Å	I/I_0	hkl	d_{hkl}/Å	I/I_0	hkl
12.007	20	002	11.466	14	002	11.612	35	002	11.510	17	002
9.729	38	111	9.435	37	111	9.620	91	111	9.536	49	111
8.372	100	020	8.399	100	020	8.918	100	020	8.801	100	020
7.961	5	112	7.679	3	112	7.815	2	112			
						7.375	2	120			
6.866	10	022	6.766	12	022	7.070	29	022	6.994	15	022
6.866	10	200	6.566	3	200	6.552	5	200	6.512	2	200
						6.299	3	201			
6.385	4	113	6.145	4	113	6.239	9	113	6.192	5	113
									5.758	1	004
5.965	4	202	5.696	3	202	5.704	7	202	5.670	2	202
						5.615	2	014			
			5.391	1	212	5.433	6	212	5.396	2	212
5.313	2	220	5.171	3	220						
5.057	5	131	5.022	1	131	5.272	32	131	5.208	18	131
5.206	3	221				5.148	3	221			
						5.086	3	114			
						4.998	5	203			
						4.900	8	132			
						4.862	10	024	4.817	4	024
4.865	3	222	4.714	6	222	4.805	9	222	4.765	6	222
4.340	3	133	4.268	4	133	4.436	15	133	4.389	12	133
4.184	1	040	4.194	8	040	4.454	18	040	4.395	14	040
									4.315	2	404
									4.267	1	301
						4.247	3	310	4.214	1	310
						4.168	5	042			
						4.148	1	311			
						4.153	7	034	4.109	4	034
3.9525	3	141	3.9361	3	141	4.153	7	141	4.098	4	141
			3.9834	2	232	4.112	3	232	4.074	3	232
			3.8423	1	125	3.9231	2	320	3.8927	1	320
3.9824	1	006	3.8189	2	006	3.8664	5	006	3.8398	3	006
						3.8248	1	233			
			3.7564	1	205	3.7874	1	205			
3.8628	3	313	3.6992	3	313	3.7191	12	313	3.6992	3	313

space group as the $A_2Sn_3Se_7$ member ($P2_12_12_1$). The measure of the goodness-of-fit between the observed and calculated d-spacings for the first 35–55 reflections, $|\Delta 2\theta|=0.005$ Å, is excellent.

Comparison between the diffraction data in the two left hand columns of Table 1, reveals the structural identity between both $TMA_2Sn_3S_7$ and $TMA_2Sn_3Se_7$ materials. The only difference is related to a significant enlargement of the lattice of the selenide owing to the greater size of Se^{2-} compared to S^{2-}. Despite the lattice metric differences, both samples provide almost identical sets of *hkl* reflections, matching even their intensities. These data are interpreted as direct confirmation that the two materials are unequivocally isostructural.

The next step is to confirm the structural identity between the three SnS-1 materials with different templates. From the data in Table 1 the effect of the second structural component, different A^+, is clear. One can see the dramatic expansion of the interlayer spacing by up to 0.9 Å (b parameter) for QUIN-SnS-1, containing the largest template cation of all three, Table 2, while a and c are changed slightly (0.1 and 0.3 Å, respectively). Another interesting result, directly related to the effect of the template on the structures of SnS-1 materials, is the surprisingly sharp increase of the total number of diffraction peaks observed on passing from TMA-SnS-1 to TBA-SnS-1 to QUIN-SnS-1, Table 1. The largest number of reflections emerge for the material with the largest organic template, QUIN-SnS-1. The reason for this cannot be simply the enlargement of the unit cell, as TMA-SnSe-1 having a larger unit cell volume than QUIN-SnS-1, provides considerably fewer diffraction peaks. Possible reasons for this interesting effect could be either the diffraction contribution of the template itself, the symmetry of the template, and/or some framework changes, caused by its organization within the structure. This could originate from a tighter attachment of the larger QUIN to the framework, improving the overall structural order.

Thermal stability of SnS-1

Variable temperature powder X-ray diffraction (VTPXRD) study of the thermal stability under a nitrogen atmosphere. The three analyzed materials exhibit changes in their lattice dimensions when they are heated under a N_2 atmosphere. Table 3 shows the lattice parameters for each sample calculated at 25 °C and at the highest temperature at which the basic set of *hkl* reflections, Table 1, could be measured with reliable accuracy. These structures are found to collapse at the following temperatures: TMA-SnS-1 at 250 °C, QUIN-SnS-1 near 300 °C and TBA-SnS-1 below 250 °C. All these data are in agreement with the results from TG data obtained for the same three samples (see later). Despite some small discrepancies, likely due to different heating rates, TBA-SnS-1 was found to be the least stable material by both techniques. *In situ* VTPXRD

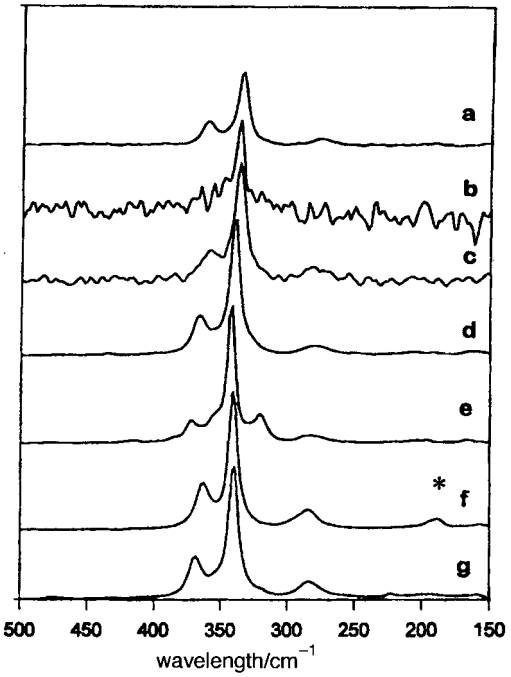

Fig. 1 Raman vibrational spectra of various SnS-1 structure types showing the tin–sulfur skeletal fingerprint region. Organic cations are: (a) tetramethylammonium, (b) quinuclidinium, (c) *tert*-butylammonium, (d) piperidinium, (e) $DABCOH^+$, (f) hexane-1,6-diammonium, (g) pyrrolidinium. The asterisk denotes a tin impurity.

Table 2 Organic cations employed as void fillers for SnS-1 with volumes calculated using the method of Connolly[22]

organic cation	V/Å^3
tetramethylammonium	80
quinuclidinium	104
tert-butylammonium	80
pyrrolidinium	70
hexane-1,6-diammonium	121
piperidinium	84
diazobicyclooctanammonium	103

analysis shows a continuous change of the lattices, gradually losing crystallinity before the eventual collapse of the structure. The QUIN-SnS-1 material shows an increase of the lattice dimensions in all three directions, while the other two materials exhibit a contraction of the unit cells. The values of a particular lattice dimensional change, Δ are shown in Table 3. These values for TMA-SnS-1 and QUIN-SnS-1 are quite small for a, b and c (0.02–0.13 Å).

Sample TBA-SnS-1 is unusual compared to TMA-SnS-1 and QUIN-SnS-1. From the very beginning of the heating, at 50 °C, it exhibits a dramatic decrease of the interlayer spacing ($\Delta b = -1.54$ Å, or 9.1% of b and $\Delta c = -0.8$ Å, or 3.3% of c). This phenomenon could be due to some TBA rearrangement in the interlayer space. After this initial contraction, the structure and the lattice dimensions remain stable up to the collapsing point. Note that the drastic change of the lattice volume (up to 8%) does not correspond to any chemical event or mass loss detected by TG analysis (see later). This supports the assumption that the one-dimensional lattice change could originate from rearrangement of the template from the interlayer to the micropore void space, such that the integrity of the structure remains unchanged.

Variable temperature powder X-ray diffraction study of thermal stability under vacuum. The same SnS-1 materials were heated using the same experimental conditions (sample preparation, data collection, heating rate), but under vacuum, Fig. 2. Under vacuum most of these compounds exhibit a greater thermal stability compared to under nitrogen. For the analyzed samples, the collapsing point was shifted towards higher temperatures: $\Delta T = 100$ °C for QUIN-SnS-1, $\Delta T = 75$ °C for TMA-SnS-1 and $\Delta T = 40$ °C for TBA-SnS-1. This is related to the constant removal of evolved molecules from the structure during heating, minimizing any chemical reactions that can degrade the framework.

The unit cell parameters for all three samples at temperatures close to the collapsing point are found to be very similar to those obtained under nitrogen. While the thermal behavior of the analyzed materials under vacuum did not show any unexpected changes, a direct comparison between the unit cell parameters of these samples at room temperature in air and under vacuum revealed some valuable information about the effect of water molecules and/or the organic templates in these structures, Table 4. TMA-SnS-1 and QUIN-SnS-1 show a quite small change, while the interlayer space of TBA-SnS-1 shrinks in a dramatic way along b, with $\Delta b = -1.33$ Å.

Effect of applied pressure on SnS-1

In order to form self-supported wafers of the materials, the effect of the pressure placed on the materials by the die employed was investigated, with surprising results. Portions of the same TBA-SnS-1 sample were pressed for about a minute at the pressures indicated in Fig. 3(a)–(d). Changes in the PXRD pattern were observed and the distinctive odour of *tert*-butylamine and hydrogen sulfide increased with applied pressure. The PXRD pattern continued to change with the length of time of the applied pressure and was found to be partially reversible upon releasing the pressure and leaving the sample in air, Fig. 3(e),(f). The extent of reversal was greatest for samples treated at lower pressure. Exposure of the samples to *tert*-butylamine was not found to assist this relaxation process. The new PXRD reflections grow in with unchanging position for increasing applied pressure. They bear a relation to the original peaks as indicated in Fig. 3. These observations are consistent with the pressure-induced removal of some *tert*-butylamine void filler and sulfur from the SnS-1 lattice causing a change in the symmetry, stoichiometry, degree of amine occlusion and phase purity of the material.

QUIN-SnS-1 was pressed under 500 kg (*ca.* 2260 psi) and remained unchanged, Fig. 4. This establishes that the frame-

Table 3 Lattice changes of different $A_2Sn_3S_7$ materials in a N_2 atmosphere

sample, T/°C	a/Å	b/Å	c/Å	V/Å^3
TMA, N_2, 25 °C	13.074(4)	16.774(5)	22.821(13)	5004(2)
TMA, N_2, 200 °C	13.001(8)	16.658(7)	22.694(19)	4917(4)
Δ(%)/Å	−0.072(0.6)	−0.116(0.7)	−0.127(0.6)	−87(1.7)
QUIN, N_2, 25 °C	13.089(3)	17.864(6)	23.181(5)	5420(2)
QUIN, N_2, 250 °C	13.182(3)	17.886(4)	23.233(4)	5478(1)
Δ(%)/Å	+0.093(0.7)	+0.022(0.1)	+0.052(0.2)	+58(1.1)
TBA, N_2, 25 °C	12.977(7)	17.473(7)	23.877(15)	5187(3)
TBA, N_2, 150 °C	13.002(9)	15.933(7)	23.102(16)	4786(3)
Δ(%)/Å	+0.025(0.2)	−1.540(9.1)	−0.775(3.3)	−401(7.9)

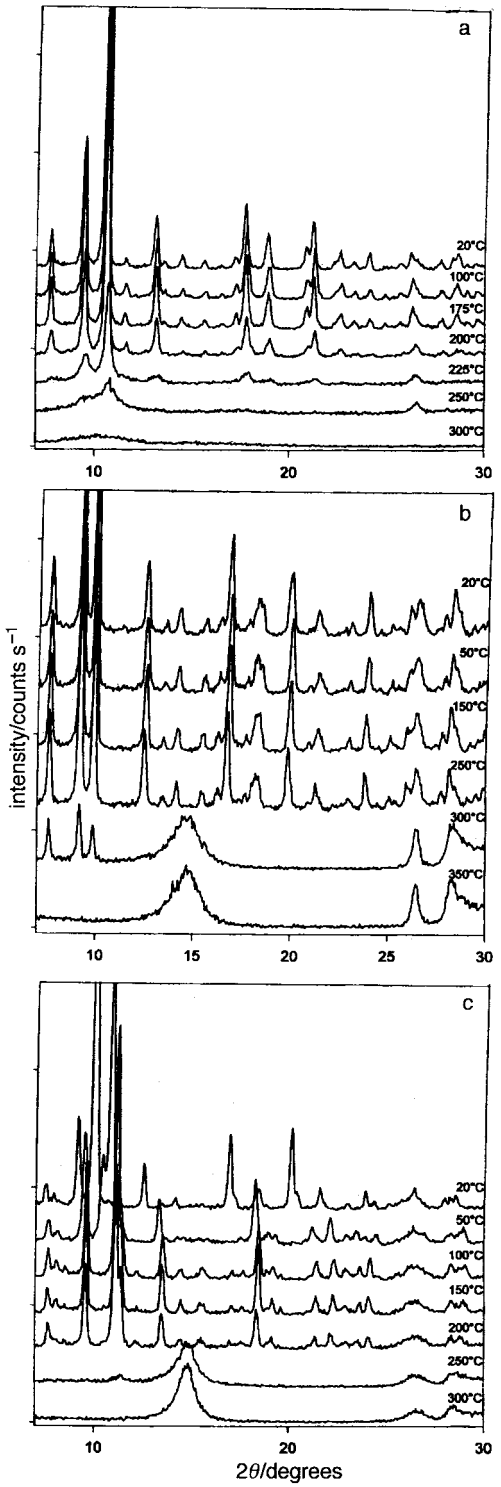

Fig. 2 High temperature powder X-ray diffraction data collected under flowing nitrogen for (a) TMA-SnS-1, (b) QUIN-SnS-1, (c) TBA-SnS-1. The temperature at which each pattern is collected is indicated.

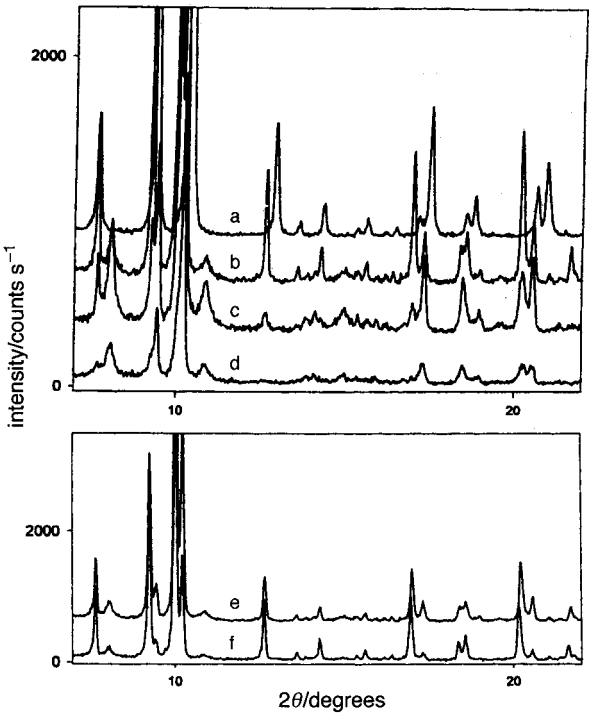

Fig. 3 Powder X-ray diffraction data for TBA-SnS-1, (a) as synthesized, and after having been pressed at (b) 600 kg (2700 psi), (c) 1200 kg (5400 psi), and (d) 4800 kg (21700 psi). Lower figure shows same material pressed at (e) 300 kg (1400 psi) and (f) relaxation following pressing at 300 kg.

work is stable to applied pressure in contrast to TBA-SnS-1. This may be a reflection of the size and rigidity of the template cation. The Connolly surfaces of the templates[22] show that quinuclidinium is the largest of the cations used in this study: QUIN = 104 Å^3, TMA = 80 Å^3, TBA = 80 Å^3. In addition, the minimal mass loss below 100 °C seen in the TG of QUIN-SnS-1 indicates that there is little water within the structure. These observations imply that quinuclidine is sufficiently large and rigid to effectively brace the structure against contraction and is sufficiently involatile to retain its pillaring function. This is in keeping with the thermal stability data which showed QUIN-SnS-1 as the most thermally stable and inflexible of the three structures.

Thermogravimetry

Thermogravimetry (TG) of SnS-1, in conjunction with the results of VTPXRD, provide insight into the stability of the structure with respect to template removal. Fig. 5 shows the thermal data for each of the three materials recorded under nitrogen. The largest mass loss occurs at a slightly lower temperature than under vacuum. TBA-SnS-1 is seen as the least thermally stable, having its greatest loss by 275 °C, while for TMA-SnS-1 and QUIN-SnS-1 this loss is at higher temperatures, *ca.* 300 and 350 °C, respectively. Both TBA-SnS-1 and QUIN-SnS-1 show single events at these temperatures while

Table 4 Lattice changes of different $A_2Sn_3S_7$ materials under vacuum

sample, T/°C	a/Å	b/Å	c/Å	V/Å^3
TMA, air, 25 °C	13.102(7)	16.851(6)	22.984(15)	5074(3)
TMA, vac., 25 °C	13.028(7)	16.713(7)	22.795(15)	4964(3)
Δ(%)/Å	−0.074(0.6)	−0.138(0.8)	−0.189(0.8)	−116(2.3)
QUIN, air, 25 °C	13.088(5)	17.858(7)	23.172(8)	5416(3)
QUIN, vac., 25 °C	13.124(4)	17.714(6)	23.214(8)	5397(2)
Δ(%)/Å	+0.036(0.3)	−0.144(0.8)	+0.042(0.2)	−19(0.3)
TBA, air, 25 °C	13.020(4)	17.576(4)	23.021(5)	5268(2)
TBA, vac., 25 °C	13.047(5)	16.247(5)	23.418(7)	4964(3)
Δ(%)/Å	+0.027(0.2)	−1.329(7.6)	+0.397(1.7)	−304(5.8)

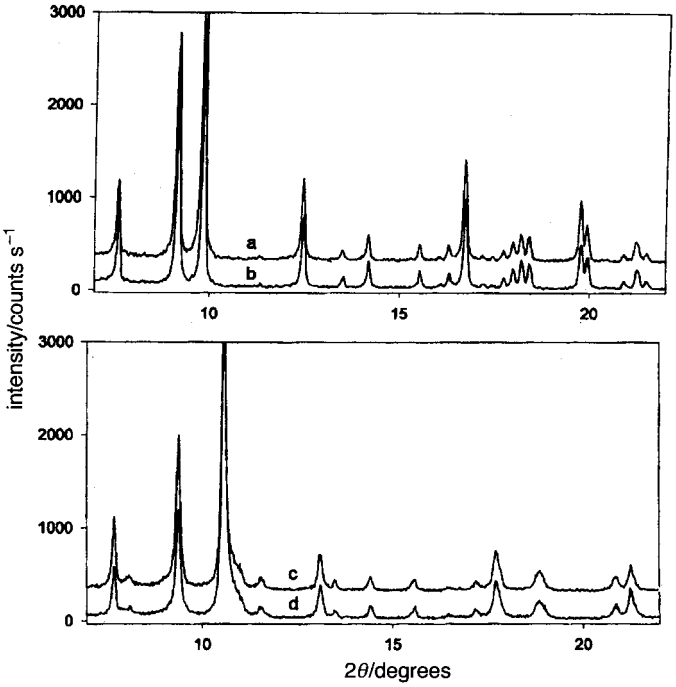

Fig. 4 Powder X-ray diffraction patterns (a) QUIN-SnS-1 as synthesized and (b) QUIN-SnS-1 after having been pressed at 500 kg (2300 psi), (c) TMA-SnS-1 as synthesized and (d) TMA-SnS-1 after having been pressed at 500 kg

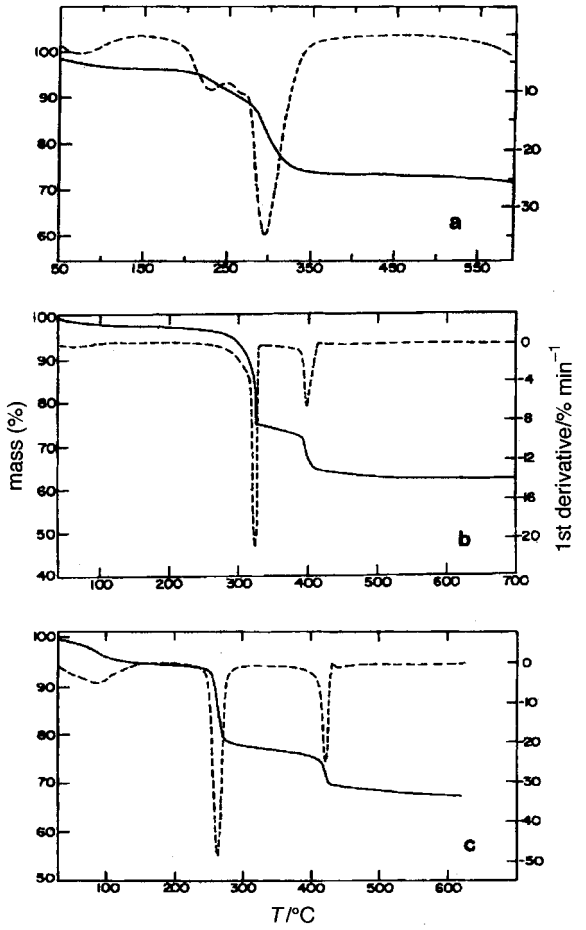

Fig. 5 Thermogravimetric data for (a) TMA-SnS-1, (b) QUIN-SnS-1 and (c) TBA-SnS-1. Each was recorded at heating rates of 5 °C min^{-1} under flowing nitrogen.

the mass loss of TMA-SnS-1 is clearly more complicated. TMA-SnS-1 and TBA-SnS-1 show significant losses before reaching 100 °C, while QUIN-SnS-1 does not. Some patterns also showed a higher temperature event at *ca.* 440 °C. All of the materials showed some further mass losses at temperatures > *ca.* 700 °C, corresponding to the formation of a mixture of berndtite (SnS_2), herzenbergite (SnS) and cassiterite (SnO_2).[4] All of these observations are in reasonable agreement with the variable temperature PXRD data.

Combined thermogravimetry and mass spectrometric analysis

The technique of TG is especially powerful when combined with mass spectrometry. The technique of mass spectrometry of porous solids has been previously described, as applied to aluminophosphate materials.[19] Fig. 6 shows the TG data for TMA-SnS-1 in combination with the mass spectrum taken at the maximum of the total ion chromatograph. At temperatures below *ca.* 175 °C, virtually no ions above *m/z* 28 (dinitrogen) are detected indicating that the mass loss below this temperature is most likely water, which is confirmed by mass spectrometry. In the regions of the early mass loss, the ion chromatograph shows primarily the cracking products of trimethylamine and dimethyl sulfide together with some recombination or products of redox reactions that occur late in the main body of the mass loss. These observations are summarised below:

m/z	ion
47	SCH_3^+
58	$(CH_3)_2NCH_2^+$
59	$(CH_3)_3N^+$
62	$(CH_3)_2S^+$
79	$(CH_3)SS^+$
94	$(CH_3S)_2^+$

These observations suggest the following decomposition reaction:

$$[(CH_3)_4N]_2Sn_3S_7 \rightarrow 2\ (CH_3)_3N + (CH_3)_2S + 3\ SnS_2 \quad (1)$$

Looking quantitatively at the TG results, the first loss attributed to water represents 2% by mass of the remaining material, corresponding to 1.6 molecules per pore. Taken separately, the main losses represent 6 and 18%, but given that during both events the primary products (*e.g.* *m/z* 47 = SCH_3^+) are present they are better taken together. The value of 24% agrees very well with the loss, 25%, expected from the above decomposition reaction. The predominance in the mass spectrum of the CH_3SSCH_3 species at *m/z* = 94 over the CH_3SCH_3 species at *m/z* = 62, however, along with previously published data regarding the high temperature reactions of SnS-1 materials,[4] suggest a second process occurring during the higher-temperature region of the mass loss. Supposing the low temperature reaction occurs partially and according to:

$$[(CH_3)_4N]_2Sn_3S_7 \rightarrow (CH_3)_3N + 0.5\ CH_3SCH_3 + (CH_3)_4NSn_3S_{6.5} \quad (2)$$

it might be followed by a high temperature process involving the reduction of tin and oxidation of sulfur observed previously:[4]

$$(CH_3)_4NSn_3S_{6.5} \rightarrow (CH_3)_3N + 0.5\ CH_3SSCH_3 + 3\ SnS_x\ (x = 1,\ 1.5,\ 2) \quad (3)$$

giving an overall thermal loss equation:

$$[(CH_3)_4N]_2Sn_3S_7 \rightarrow 2\ (CH_3)_3N + 0.5\ CH_3SCH_3 + 0.5\ CH_3SSCH_3 + 3\ SnS_x \quad (4)$$

where $x = 1,\ 1.5,\ 2$. While this agrees less well with the

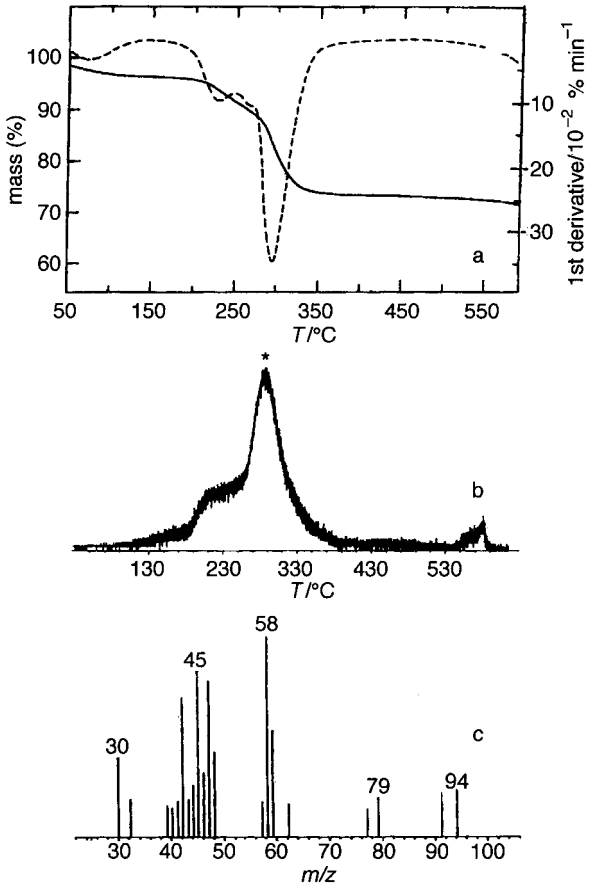

Fig. 6 (a) Thermogravimetric data for TMA-SnS-1; (b) total ion chromatograph; and (c) mass spectrum at the maximum of the ion chromatograph, as indicated with an asterisk in (b)

quantitative TG results, it is more in keeping with the intensity observed for the $m/z = 94$ species in the mass spectrum, so it is likely that both events have some part in the overall process.

When these techniques were applied to the other two materials, somewhat different results were obtained. As was noted earlier, both TBA-SnS-1 and QUIN-SnS-1 have very sharp thermal events at the template removal stage. By comparison with the TMA-SnS-1 template removal, the amine-based materials may be expected to undergo the following process:

$$[\mathrm{QUINH}]_2\mathrm{Sn_3S_7} \rightarrow 2\ \mathrm{QUIN} + \mathrm{H_2S} + 3\ \mathrm{SnS_2} \qquad (5)$$

The mass spectrometry data collected for QUIN-SnS-1 corresponds well to this mechanism. All of the significant lines present are assignable either to quinuclidine[23] or hydrogen sulfide. It is interesting that early in the first mass loss, when the framework integrity is expected to remain, quinuclidine is found to escape the framework intact. The average total loss from the two major events, 31.9%, is also in exact agreement with the proposed mechanism.

Very similar results were obtained with TBA-SnS-1. All the lines in the mass spectrum can be assigned to *tert*-butylamine[24] or hydrogen sulfide. The TG shows two events similar to those of QUIN-SnS-1, occurring at approximately the same temperatures. There is a far greater loss before 100 °C assigned to volatile species, more than 5% by mass. In this case, water is a component but the mass spectrum shows *tert*-butylamine desorbing as well. This is in contrast with QUIN-SnS-1 and may reflect a larger void volume filled with occluded neutral organics or water owing to the smaller size of the *tert*-butylammonium. Two events were observed, and the average total mass loss, 27%, was compared to the loss of 25% expected for the removal of organic and hydrogen sulfide. It was also noted that while the ion chromatograph for the major peak of *tert*-butylamine, at $m/z = 58$, extended only until 400 °C, that of H_2S, at $m/z = 34$, reached well beyond this point, beyond 500 °C. This may be interpreted by considering the proposed mechanism of template removal. Each *tert*-butylamine leaving the lattice will leave behind the charge balancing proton:

$$[\mathrm{Bu^tNH_3}]_2\mathrm{Sn_3S_7} \rightarrow 2\ \mathrm{Bu^tNH_2} + \mathrm{H_2Sn_3S_7} \qquad (6)$$

$$\mathrm{H_2Sn_3S_7} \rightarrow \mathrm{H_{2-2}}_x\mathrm{Sn_3S_{7-}}_x + x\ \mathrm{H_2S} \qquad (7)$$

$$\mathrm{H_{2-2}}_x\mathrm{Sn_3S_{7-}}_x \rightarrow (1-x)\ \mathrm{H_2S} + 3\ \mathrm{SnS_2} \qquad (8)$$

In order for the sulfur to be removed, two protons are required for each sulfur to form the volatile hydrogen sulfide seen in the mass spectrum. Early in the measurement this likely occurs rapidly owing to the close proximity of framework protons, but later it must be more difficult as protons must diffuse from greater distances.

Aqueous ion exchange

Traditional ion exchange is usually accomplished by repeatedly suspending the solid in an aqueous solution of the exchange ions and allowing the system to come to equilibrium. Ion exchange of this type has been claimed for SnS-1, but specific results have been lacking.[2b] Aqueous ion exchange was attempted with TBA-SnS-1 and 0.1 M TMACl. The technique of mass spectrometry was applied to ascertain the identity of the charge balancing cations. Fig. 7 shows the mass spectrum of the product resulting from one such experiment. The spectrum agrees very well with that of TMA-SnS-1, including the total ion chromatograph. For example, the peaks at $m/z = 79$ and 94, described earlier with respect to TMA-SnS-1, and never seen in TBA-SnS-1 analysis, are very strong in the spectrum of the ion-exchanged product. It certainly suggests that the TMA cations are charge-balancing. Support for this proposal stems from the PXRD pattern of the TBA-SnS-1 sample following exposure to the 0.1 M aqueous solution of TMACl. It shows that ion exchange of TBA^+ by TMA^+ has indeed occurred and that the framework integrity of the TMA-SnS-1 product has been retained intact.

Amine exchange

These exchanges were carried out by bubbling a carrier gas through the desired amine and over a shallow bed of TBA-SnS-1 to an aqueous trap. Success was judged on the basis of the mass spectrum and PXRD of the product. Four amine exchanges were attempted: trimethylamine, triethylamine, tripropylamine and *sec*-dibutylamine. These were chosen according to two criteria: size and basicity. It was supposed that if

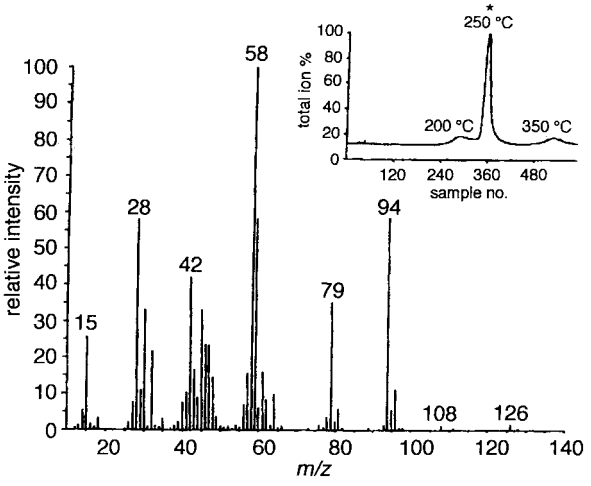

Fig. 7 Mass spectrum of TMA-exchanged TBA-SnS-1 at the peak of the total ion chromatograph, indicated in the insert with an asterisk

Table 5 Amine exchange in TBA-SnS-1

amine	pK_b[24,25]	kinetic diameter[a]	experimental result
tert-butylamine	3.17	*ca.* 6.5	
trimethylamine	4.19	*ca.* 6.5	little exchange
triethylamine	2.77	*ca.* 7.5[b]	significant exchange
tripropylamine	3.45	*ca.* 8.5	no exchange
sec-dibutylamine	2.90	*ca.* 8.0	no exchange

[a]Estimated from Connolly surfaces (ref. 22). [b]Kinetic diameter according to ref. 26.

the TBA-SnS-1 material behaved as a molecular sieve, it should exclude larger molecules rather than swelling to accommodate them. Also, a weaker base ought not to displace a stronger base. The results are summarized in Table 5.

It was found that a larger less basic amine, such as tripropylamine, failed to displace *tert*-butylamine, as indicated by the absence of a measurement of any species of $m/z = 114$, characteristic of that amine. PXRD shows little change in the crystallinity of the material but there was a shift to slightly lower *d*-spacings, corresponding, to *ca.* 2% decrease in layer spacing ***b***, with negligible change in ***a*** or ***c***. Tripropylamine was very clearly excluded.

A more basic but much larger amine, *sec*-dibutylamine, also failed to significantly exchange as seen by the absence of any species at $m/z = 100$ above 100 °C (after the removal of any surface physisorbed species). However, the powder pattern shows a significant loss of crystallinity. The mechanism of this loss of crystallinity is not clear. The data imply exclusion of the much larger amine. Trimethylamine, an amine slightly smaller than *tert*-butylamine, may have achieved some limited displacement, despite its lesser basicity, indicated by an increased intensity in the parent-ion peak at $m/z = 59$. Again, a loss of crystallinity was observed.

Finally, the exchange with triethylamine, a more basic and significantly larger amine although smaller than *sec*-dibutylamine, was found to successfully occur without damage to the lattice. The MS shows the dominant peak at $m/z = 86$ characteristic of triethylamine, and it remains to high temperature indicating the triethylamine is truly exchanged. Success was also obtained when the TBA-SnS-1 powder was slurried with neat triethylamine. The reduced intensity of the parent ion peak at $m/z = 101$ indicates that substantial exchange has been achieved. PXRD indicated a significant expansion of the lattice, where the primary expansion is 0.36 Å in ***b***, reflecting an increased interlayer spacing. The changes in ***a*** and ***c*** are much smaller, ***a*** decreasing by 0.17 Å and ***c*** increasing by 0.04 Å. This suggests some change in template positioning in addition to size.

These results are very interesting in terms of the original hypotheses regarding ion-exchange and intercalation by SnS-1. Here is a middle ground in which, within a certain range, the SnS-1 layers are able to swell to allow entry of a larger species. Outside this range, molecules may be excluded showing a sieving effect.

Adsorption and molecular discrimination in SnS-1

Fig. 8 shows adsorption isotherms for TMA-SnS-1 with several gases, H_2O, CO_2, N_2 and Ar at the temperatures indicated. The sample was dehydrated at 120 °C under high vacuum to remove water. These adsorption data provide considerable insight into the molecule sieving/intercalation issue. The adsorption of CO_2 follows a regular type I isotherm. This is typical of a microporous solid having very little external surface area relative to the internal surface area. The large initial uptake at low partial pressure is limited by the micropores within the structure; any further uptake in the latter part of the curve corresponds to adsorption on the external surface.[25]

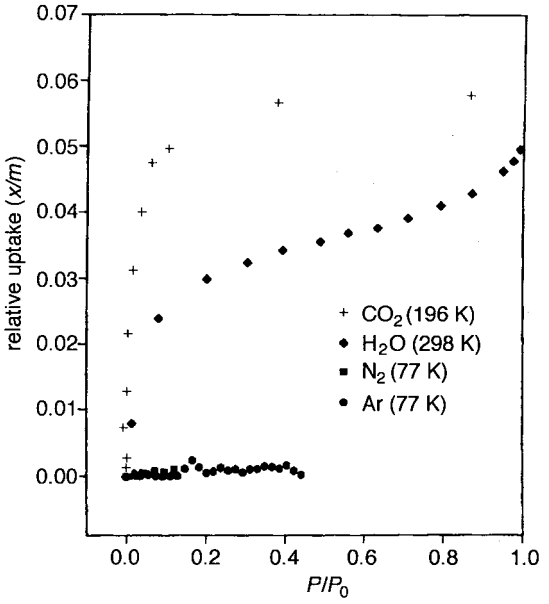

Fig. 8 Adsorption isotherms for TMA-SnS-1 showing the uptake of H_2O and CO_2 and the exclusion of Ar and N_2, at the temperatures indicated

If, instead, the materials were capable of intercalating these gases through the swelling of the interlayer spacing, a different type of isotherm would be expected, for example, a type IV isotherm. Following the micropore filling observed in the type I isotherm, gas uptake should be further enhanced as the material begins to swell. Finally, at some maximum expansion, the uptake might stop and any further uptake would be due to multilayer adsorption on the external surface. This is not observed for either H_2O or CO_2.

TMA-SnS-1 clearly excludes nitrogen and argon while allowing carbon dioxide and water to enter and produce the isotherms obtained. This is interesting given the difference in kinetic diameter between CO_2 (3.3 Å) and Ar (3.4 Å) is so small.[26] This appears to be obvious evidence of the sub-angstrom precision molecular sieving ability of SnS-1.

Another interesting result is that when it was attempted to collect adsorption data for CO_2 on similarly pre-treated QUIN-SnS-1, the material was found to adsorb very little gas [<0.01 mg N_2 (mg sample)$^{-1}$ at p/p_0 *ca.* 0.2], in sharp contrast to TMA-SnS-1 which was five times greater. It is believed that this is the result of the larger quinuclidine template leaving essentially no room for entry of the carbon dioxide molecule. This is entirely consistent with the TG–MS and applied pressure results for QUIN-SnS-1, showing very little water desorption and little sensitivity to pressure indicative of a large, rigid, space-filling void filler.

It was possible to calculate the pore volume from the CO_2 adsorption data, using a Dubinin plot.[27] This gives an accessible pore void volume of 0.04 cm^3 g^{-1} which may be compared to void volumes obtained for zeolites. For example, the void volume of NaA and NaX is 0.26 and 0.31 cm^3 g^{-1}, respectively.[28] The void volume of TMA-SnS-1 is small by comparison to these values, but reasonable especially considering that all of the TMA^+ organic void filler is still remaining within the SnS-1 framework and that the molar mass of TMA-SnS-1 is greater than three times that of silica. Also, it should be remembered that zeolite X has 13 Å supercages which are almost entirely empty. The value also compares quite well with the calculated free volume accessible to CO_2, 0.07 cm^3 g^{-1}, obtained using the Connolly surface calculation.[22] The software calculates the volume occupied by the unit cell contents using CO_2 as a probe molecule, which is then subtracted from the unit cell volume. The void volume of the

hypothetical template-removed material is calculated to be 0.4 cm^3 g^{-1}.

Conclusions

The intra- and inter-layer flexibility of the microporous layered SnS-1 structure is seen through the sensitivity of the unit cell parameters to adsorbed water, template and temperature, the large number of distinct void fillers that form slightly different polymorphs, the effects of exchange of void filler as achieved with the amine treatments, and the effect of the application of pressure. It appears that the tin–sulfide trigonal bipyramidal building-blocks which create the micropores within the tin sulfide layers, can function as flexible hinge-points to give remarkable pliability to the SnS-1 structure. The materials are found to have a reasonable temperature stability, which is important with respect to the post-synthesis removal of organics. Finally, the materials are shown to have a character intermediate between the layered metal chalcogenide and oxide molecular sieves. They display sieving behaviour towards small non-polar molecules like CO_2 and N_2 while showing interlayer expansion to accommodate larger amines in the fashion of an intercalation material. All of this bodes well for future catalysis, separation and chemical sensing applications based on this class of microporous layered tin(IV) sulfides.

Appendix: Some peculiarities in the PXRD analyses of $A_2Sn_3S_7$-type materials

The powder X-ray analysis performed on these materials was a little unusual owing to some unique features of their structures. It is pointed out in the text that as a result of complex structural interactions between the three different building units, the framework becomes extremely flexible. Some of the materials exist in different polymorphic forms (TMA-SnS-1: orthorhombic and monoclinic), some of them can even undergo a structural transition at room temperature as a consequence of water absorption in air (TEA-SnS-1), some of them change under pressure (TBA-SnS-1), and most of them experience changes even after a standard powder packing procedure. One of the main characteristics of all these kinds of compounds was a surprisingly large variation in their unit cell parameters. The same kind of material, prepared under constant conditions always show quite distinctive lattice changes, reaching up to 0.8 Å per parameter, while the extremely flexible framework is still able to maintain the structure. One reason for this phenomenon could be a quite loose attachment of the $[Sn_3S_7]^{2-}$ layers with the encapsulated organic template cation and water fillers that cause not only the layer's displacement along the [010] direction, but could partially destroy the overall three-dimensional periodicity. Thus, the structure could be considered as composed of differently distorted 'clusters of layers'. The overall distribution of such 'continuously random stacking faults' could vary from crystallite to crystallite within the same material. Note that this flexibility of the framework is well supported by the appropriate space group $P2_12_12_1$ in which the lack of the mirror planes and the existence of screw axes in all three directions ensure the freedom of such types of distortions. Besides, all 20 framework atoms in the asymmetric unit $[Sn_6S_{14}]^{4-}$ are in general positions having the maximum degree of freedom. The calculated powder X-ray data lattice parameters are representing an average unit cell for a particular sample which may be different for other as-synthesized products of the same material as the statistical distribution of these defects would vary widely between the crystallites within the material. This is our explanation for the frequently observed significant differences of the unit cell parameters of the same materials (TMA-SnSe-1, for example), obtained from single crystal data (one crystal) and from powder data (bulk sample). Another effect of these steadily occurring lattice strains is an overall peak broadening, noticeable for some samples even at the low-θ range of the PXRD pattern. This abruptly decreases the total number of well resolved reflections that can be used for the lattice refinement. The result is well illustrated with the average $|\Delta 2\theta|$ values listed in Table 1 that were evaluated from the least squares refinement of the unit cell for all four materials. From 0.0163 for TMA-SnSe-1 (with 35 measured reflections), this value dropped down to 0.0049 for TBA-SnS-1 because of the sharp increase of the number of reflections (55 available within the same range on the diffraction pattern). From this point of view, TBA-SnS-1 should be considered as having the highest long range periodicity and the best layer registry compared with all analyzed materials.

The lack of well defined unit cell parameters and the relatively small number of measurable reflections were the main troubles that we encountered in the PXRD characterization of these materials. Keeping this in mind, one can consider the data in Table 1 only as reliable proof for the expected structural identity of all three A-SnS-1 materials with TMA-SnSe-1 utilized as a tool for their primary characterization, that is, structural type, purity, lattice parameters and overall defect distribution. A more detailed look at the data in the table would raise many questions relating to the complexity of the structure. The unit cell values listed in Table 1 are valid only for the particular samples for which powder X-ray data were refined in the least squares procedure, but because of their variance they could not be considered (or used) as characteristic of the SnS-1 materials.

Another experiment which is discussed in this paper is *in situ* PXRD analysis under different atmospheres and temperatures. The results listed in Tables 3 and 4 describe very well the behavior of all analyzed samples. Such experiments are performed periodically in our laboratory, and it is a common practice that, for each one of these *in situ* measurements, the best samples that are representative of each kind of A-SnS-1 material were taken from different preparations. Therefore, their initial unit cell parameters and volumes are more or less different and incomparable with the ones provided in Table 1. Even the data in Table 3 and 4 are not comparable; only the QUIN-SnS-1 sample was the same material used for both N_2–T °C (Table 3) and vacuum–T °C (Table 4) experiments, while for the two other materials, the samples analyzed in both experiments were from different syntheses. Nevertheless, the data in Tables 3 and 4 should be considered as reliable and representative of all structural changes that occur from the different treatments; the measurements were performed under strictly controlled experimental conditions, the analyses were repeated more than once and, as discussed in the text, the results obtained are in agreement with the data from other techniques.

We acknowledge the Natural Sciences and Engineering Research Council of Canada (NSERC), the Canadian Space Agency (CSA) and UOP for financial support of this endeavour. The authors are also most grateful to Dr Scott J. Kirkby for collecting the Raman spectra and to Dr Alex Young who obtained the mass spectrometry data. C. B. thanks NSERC and the University of Toronto for financial support during her graduate work.

References

1 R. L. Bedard, L. D. Vail, S. T. Wilson and E. M. Flanigen, *U.S. Pat.*, 4 880 761, 1989; R. L. Bedard, S. T. Wilson, L. D. Vail, J. M. Bennett and E. M. Flanigen, *Stud. Surf. Sci. Catal.*, 1989, **49A**, 375.

2 (*a*) H. Ahari, G. A. Ozin, R. L. Bedard, S. Petrov and D. Young, *Adv. Mater.*, 1995, **7**, 370; (*b*) J. B. Parise, Y. Ko, J. Rijssenbeek, D. M. Nellis, K. Tan and S. Koch, *J. Chem. Soc., Chem. Commun.*, 1994, 527; (*c*) K. M. Tan, Y. G. Ko and J. B. Parise, *Acta Crystallogr., Sect. C*, 1995, **51**, 398.

3 H. Ahari, C. L. Bowes, T. Jiang, A. J. Lough, G. A. Ozin, R. L. Bedard, S. Petrov and D. Young, *Adv. Mater*., 1995, **7**, 375.
4 T. Jiang, G. A. Ozin and R. L. Bedard, *Adv. Mater*., 1994, **6**, 860; 1995, **7**, 166.
5 P. Enzel, G. S. Henderson, G. A. Ozin and R. L. Bedard, *Adv. Mater*., 1995, **7**, 64.
6 G. A. Marking and M. G. Kanatzidis, *Chem. Mater*., 1995, **7**, 1915.
7 R. J. Francis, S. J. Price, J. S. O. Evans, S. O'Brien, D. O'Hare and S. M. Clark, *Chem. Mater*., 1996, **8**, 2102.
8 (*a*) C. L. Bowes, T. Jiang, A. J. Lough, G. A. Ozin, S. Petrov, G. Vovk, A. Verma, D. Young and R. L. Bedard, *Proc. 9th. Int. Symp. Molecular Recognition and Inclusion*, ed. A. Coleman, Lyon, France, November 1996, Kluwer Academic, Dordrecht, The Netherlands, 1997; (*b*) Ö. Dag, H. Ahari, N. Coombs, T. Jiang, P. Aroca-Ouellette, S. Petrov, R. L. Bedard, I. Sokolov, A. K. Verma, G. Vovk, D. Young and G. A. Ozin, *Adv. Mater*., 1997, **9,** 1131; (*c*) T. Jiang and G. A. Ozin, *Adv. Mater*.; (*d*) H. Ahari, R. L. Bedard, C. L. Bowes, N. Coombs, Ö. Dag, T. Jiang, A. Lough, G. A. Ozin, S. Petrov, A. K. Verma, G. Vovk and D. Young, *Nature* (*London*), 1997, **388,** 857.
9 A. J. Jacobson and M. S. Whittingham, in *Intercalation Chemistry*, ed. M. S. Whittingham and A. J. Jacobson, Academic Press, Toronto, 1982.
10 *Intercalation in Layered Materials*, ed. M. S. Dresselhaus, Plenum Press, New York, 1986.
11 A. A. Balchin, in *Crystallography and Crystal Chemistry of Materials with Layered Structure*, ed. F. Lévy, D. Reidel, Dordecht, Holland, 1976.
12 B. Palosz and S. Gierlotka, *Acta Crystallogr., Sect. C*, 1985, **41**, 807; 1402; 1986, **42**, 653.
13 C. A. Formstone, E. T. Fitzgerald, P. A. Cox and D. O'Hare, *Inorg. Chem*., 1990, **29**, 3860.
14 A. Leblanc, M. Danot and J. Rouxel, *Bull. Soc. Chim. Fr*., 1969, **1**, 87.
15 K. Kourtakis, J. DiCarlo, R. Kershaw, K. Dwight and A. Wold, *J. Solid State Chem*., 1988, **76**, 186.
16 D. O'Hare, W. Jaegermann, D. L. Williamson, F. S. Ohuchi and B. A. Parkinson, *Inorg. Chem*., 1988, **27**, 1537; C. A. Formstone, E. T. Fitzgerald, D. O'Hare, P. A. Cox, M. Kurmoo, J. W. Hodby, D. Lillicrap and M. Goss-Custard, *J. Chem. Soc., Chem. Commun*., 1990, 501; D. O'Hare, J. S. O. Evans, P. J. Wiseman and K. Prout, *Angew. Chem., Int. Ed. Engl*., 1991, **30**, 1156; S. M. Clark, J. S. O. Evans, D. O'Hare, C. J. Nuttall and H-V. Wong, *J. Chem. Soc., Chem. Commun*., 1994, 809.
17 W. M. Meier and D. H. Olson, *Atlas of Zeolite Structure Types*, Butterworth-Heinemann, Toronto, 3rd edn., 1992.
18 R. M. Barrer, *Zeolites and Clay Minerals*, Academic Press, New York, 1978, p. 461.
19 D. Young and A. Young, *J. Mater. Chem*., 1993, **3**, 295.
20 H. Ahari, Ö. Dag, S. J. Kirkby and G. A. Ozin, unpublished work.
21 S. Petrov, unpublished work.
22 M. L. Connolly, *Science*, 1983, **709**, 221; *J. Appl. Crystallogr*., 1983, **16**, 548.
23 NBS Library of Mass Spectra.
24 *Eight Peak Index of Mass Spectra*, Mass Spectrometry Data Centre, Reading, UK, 1st edn., 1970, vol. 1.
25 K. S. W. Sing, D. H. Everett, R. A. W. Haul, L. Moscou, R. A. Pierotti, J. Rouquerol and T. Siemeiniewska, *Pure Appl. Chem*., 1985, **57**, 603.
26 D. W. Breck, *Zeolite Molecular Sieves*, Wiley, Toronto, 1974, p. 636.
27 S. J. Gregg and K. S. W. Sing, in ref. 26, p. 224.
28 D. W. Breck, in ref. 26, p. 436.

Paper 7/06278H; *Received* 27*th August*, 1997